

1. Experimental analysis and numerical simulation

Three grayscale images “Brain”, “Barbara”, “Cameraman” are selected as the plain images. Each is first encrypted and then embedded into color carrier images “2.2.02”, “2.2.01”, “4.2.03”. The corresponding output is described in Fig. 1. As observed, the encryption successfully obscures all recognizable details of the plain images. Additionally, the cover and corresponding ciphertext images appear visually similar, with no obvious traces of the embedded content, demonstrating strong concealment and high imperceptibility.

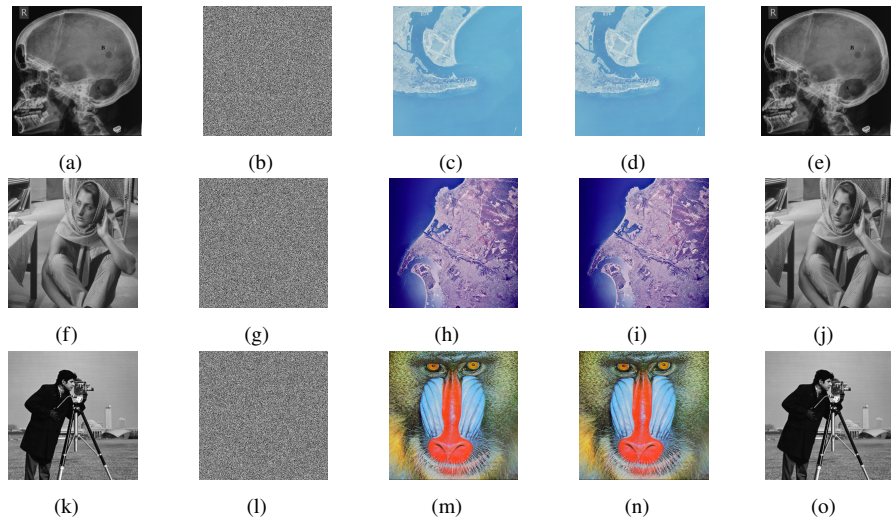


Figure 1: Visual analysis: first column represent plaintext images “Brain”, “Barbara”, “Cameraman”; second column depicts encrypted (secret) images; third column illustrate carrier images “2.2.02”, “2.2.01”, “4.2.03”; fourth column represents visually secure ciphertext (stego) images; fifth column described reconstructed (extracted) images.

1.1. Histogram analysis

This subsection assesses the encryption and concealment capabilities of the proposed algorithm using histogram analysis, as shown in Figure 2. The plain image histogram reveals distinct pixel patterns, whereas the encrypted variant depicts a uniform distribution, indicating effective diffusion [50]. Consequently, the histograms of cipher images closely resemble those of their carriers, so validating effective concealment.

Furthermore, the (χ^2) test has been conducted to validate the uniformity of the histogram of the encrypted images [5]. A significance level of 0.05 was selected

Table 1: χ^2 outcomes for images at significance level ($\alpha = 0.05$)

Theoretical Values [51]				
$\chi^2_{0.05(255)} = 293.2478$ $\chi^2_{0.01(255)} = 310.4574$ $\chi^2_{0.1(255)} = 284.3359$				
Images	Size	Initial images	Encrypted images	Output
Boats.512	512×512	435888.3417	249.7461	Pass
Lena	512×512	160421.8359	233.1184	Pass
Peppers	512×512	138836.1738	248.9060	Pass
Baboon	512×512	187598.9082	243.3320	Pass
Barbara	512×512	144101.1191	223.8691	Pass
Cameraman	512×512	418530.14648	228.9062	Pass
Girlface	256×256	715065.9375	247.4512	Pass
Cameraman	256×256	110973.3046	247.4512	Pass
Lena	256×256	30665.7031	196.0781	Pass

for this analysis. The following formula applied in this analysis is:

$$\chi^2 = \sum_{i=0}^n \frac{(x_i - y_i)^2}{y_i} \quad (1)$$

where $y_m = \frac{MN}{256}$ and x_m represents the expected and calculated frequencies respectively of each possible pixel value in the image, for $m = 0, 1, 2, 3, 4, 5, \dots, 255$ maximum pixel intensity. Table 1 presents the computed (χ^2)-values for both plain and encrypted images. The results demonstrate that the images encrypted using the proposed algorithm successfully pass the (χ^2)- test, as all calculated (χ^2)-values are lower than the corresponding critical values.

1.2. Visual quality analysis

The Peak Signal-to-Noise Ratio (PSNR) is a commonly employed statistic for evaluating the quality of a stego image relative to its original host. The PSNR is mathematically defined as follows:

$$\text{PSNR} = 20 \log \left(\frac{255\sqrt{3 \times 2^{2m}}}{\sum_{u=0}^{2^m-1} \sum_{v=0}^{2^m-1} \sum_{w=0}^3 [H(u, v, w) - W(u, v, w)]^2} \right) \quad (2)$$

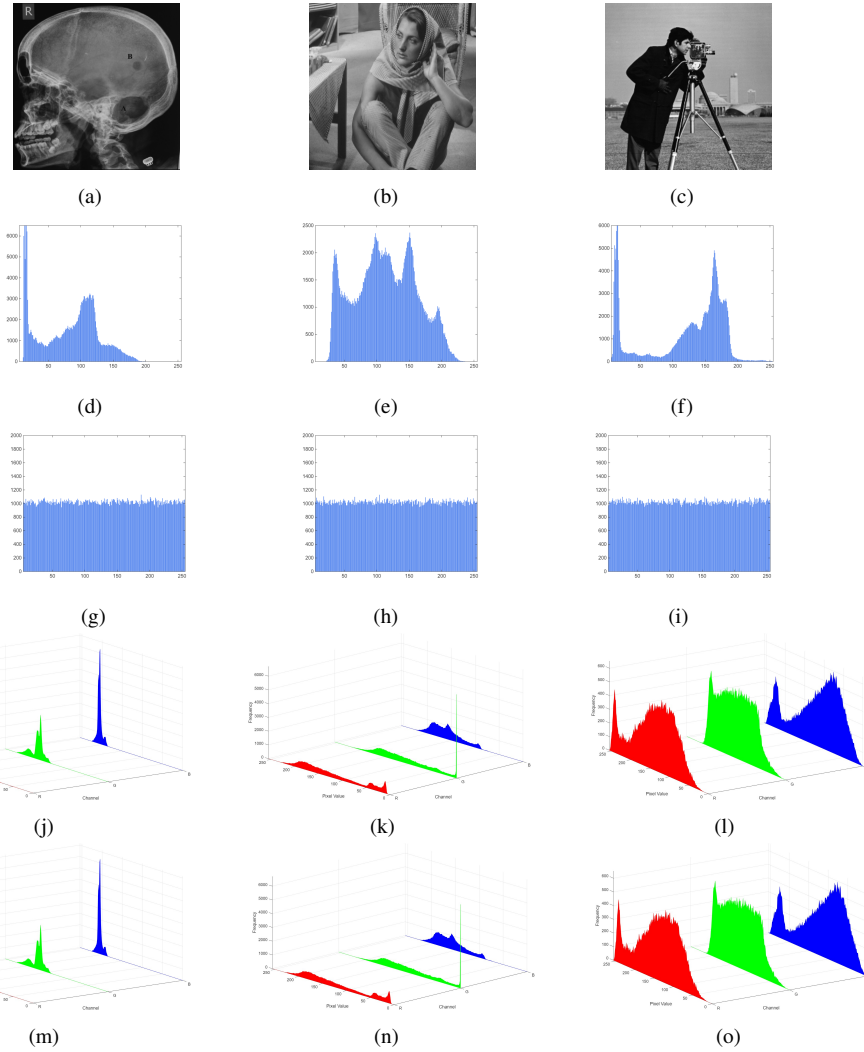


Figure 2: Histogram analysis: first row represent plain images “Brain”, “Barbara”, “Cameraman”; second row depicts histogram of plain images; third row illustrate encrypted images histogram; fourth row represents cover images “2.2.02”, “2.2.01”, “4.2.03” histogram; fifth row described ciphertext (stego) images histogram.

The seven color host images employed in this study, as enumerated in Table 2, attain PSNR values specified in the Table 2 when embedded with different secret images. As illustrated in Figure 1 and supported by Table 2, the steganographic embedding process does not produce any visually perceptible variations to the host images. The resulting embedded images demonstrate an average PSNR of approximately 54 dB, validating their high visual fidelity. As illustrated in Table 3, the PSNR metric achieved by our proposed algorithm is higher than in previous schemes approximately (around 50 dB) in [52], (around 49 dB) in [53], and (around 51 dB) in [54] while lower than the (around 55 dB) determined in [55]. To complement the extensively used PSNR metric for image quality evaluation, the Structural Similarity Index Measure (SSIM) and Normalized Cross-Correlation (NCC) are commonly utilized to assess structural similarity and image correspondence. The SSIM is characterized by the following formulation:

$$\text{SSIM}(p, q) = \frac{(2\mu_p\mu_q + I_1)(2\sigma_{pq} + I_2)}{(\mu_p^2 + \mu_q^2 + I_1)(\sigma_p^2 + \sigma_q^2 + I_2)} \quad (3)$$

Therein, μ_p, μ_q represent the mean intensity (average brightness) of the two images, while σ_p, σ_q denote their standard deviations (contrast). The term σ_{pq} is the covariance between the images, and I_1 and I_2 are small constants introduced to prevent division by zero and ensure computational stability.

The NCC measures the overall linear correlation between two images and is extensively utilized in image matching and quality assessment. NCC is hereby defined as:

$$\text{NCC} = \frac{\sum_{u=0}^{m-1} \sum_{v=0}^{m-1} s(u, v) \hat{s}(u, v)}{\sqrt{\sum_{u=0}^{m-1} \sum_{v=0}^{m-1} s(u, v)^2 \cdot \sum_{u=0}^{m-1} \sum_{v=0}^{m-1} \hat{s}(u, v)^2}} \quad (4)$$

Here $s(u, v), \hat{s}(u, v)$ depicts the pixel values of host and the steganographic image at coordinate (u, v) . As demonstrated in Table 2, the SSIM and NCC metrics for this scheme are both approximately 0.99, indicating that the embedded image preserves high visual fidelity and exhibits a strong structural resemblance to the original.

Table 2: PSNR(dB) and SSIM outcomes proposed algorithm.

Plain Images	Host images	PSNR_{cip} (dB)	SSIM_{cip}	NCC
Brain	2.2.01	54.1551	0.9998	0.996
	2.2.02	53.1334	0.9996	0.997
	2.2.05	54.1101	0.9997	0.992
Barbara	2.2.01	54.1224	0.9997	0.996
	2.2.02	53.1594	0.9998	0.995
	2.2.05	54.1408	0.9995	0.996
Women	2.2.01	54.0054	0.9998	0.997
	2.2.02	54.1074	0.9998	0.995
	2.2.05	54.1884	0.9997	0.998
Girlface	4.2.03	54.1969	0.9996	0.994
	4.2.05	54.1161	0.9998	0.996
	4.2.06	54.1919	0.9997	0.993
Lena	4.2.03	54.1296	0.9997	0.995
	4.2.05	54.1506	0.9997	0.993
	4.2.06	54.1119	0.9996	0.996
Cameraman	4.2.03	54.1004	0.9996	0.996
	4.2.05	54.1175	0.9996	0.995
	4.2.06	54.0969	0.9997	0.996

1.3. Information entropy

The Shannon entropy $S(R)$ of a random variable R is mathematically expressed as:

$$S(R) = - \sum_{j=0}^{U-1} p(w_i) \log_2(p(w_i)) \quad (5)$$

where U represents the total number of possible symbols in the sample space, and $p(w_i)$ denotes the probability of occurrence of symbol w_i . Table 4 presents the entropy results obtained from simulations for several original and corresponding encrypted images. The bolded values indicate that the proposed algorithm achieves entropy levels near the optimal threshold, confirming its effectiveness in enhancing unpredictability and its robustness against brute-force and statistical cryptanalysis.

Although global entropy efficiently quantifies the overall irregularity of an image, it may not identify non-uniform distributions within localized areas. Local entropy analysis overcomes this constraint by computing the average entropy across tiny, overlapping regions within the image. The LSE is determined by

Table 3: PSNR metric comparison

Algorithm	Secret image	Carrier image			
		4.2.03	4.2.05	4.2.06	4.2.07
Proposed	Cameraman	54.1004	54.1175	54.0969	54.1283
[52]	Cameraman	49.9618	49.9446	49.9305	49.9032
[53]	Cameraman	48.91921	48.9060	48.8659	48.8876
[55]	Women	54.5528	--	54.5792	--
[54]	Cameraman	50.5891	50.5613	50.5590	50.5130

calculating the mean of the information entropy values of the blocks that were randomly chosen, as described in Eq. 8.

$$L_{r,T_A}(P) = \sum_{j=1}^r \left(\frac{L(P_{A_j})}{r} \right) \quad (6)$$

where $L(P_{A_j})$ depicts the non overlapping blocks P_j . r, T_A represents the number of blocks and the number of pixels in each block respectively. Using parameters $(r, T_A) = (30, 1936)$ and applying a significance level of $\alpha = 0.001$, the expected LSE acceptance interval is $(7.901515698, 7.903422936)$. For an encrypted image to satisfy the LSE requirements, its LSE values must fall within the specified range. The results compiled in Table 5 confirm that the LSE values of the cipher images generated by the algorithm all reside within this range. This verifies that the encryption achieves a high degree of local randomness, ensuring a uniform and unpredictable distribution of pixel values in every region of the encrypted output.

1.4. Key space and Key sensitivity analysis

A fundamental requirement for designing effective and secure encryption algorithms is to ensure a sufficiently large and highly sensitive key space [51]. The key space in our algorithm mainly consists of the initial values $\{x_i(0)\}_{i=1}^3$ and the parameters a, b, c, A, k, ω of proposed mHNN model respectively, c, d parameters for the 2D semi-magic matrix and for GQAT the estimated key space is 10^8 [38]. Let us assume that the computer accuracy of the simulation platform is 10^{-15} , then the total key space is $(10^{15})^{11} \times 10^8 = 10^{173} \approx 2^{574}$ that exceeds the value of 2^{128} . It means that the proposed algorithm has large key space and exhibits sufficient resilience to withstand statistical attacks.

Table 4: Comparison of Information Entropy metrics

Image	Size	Proposed	Cipher Entropy					
			[56]	[57]	[58]	[59]	[60]	[61]
Baboon	512 × 512	7.9993	7.9990	7.9993	7.9993	7.9993	7.9878	7.9915
Peppers	512 × 512	7.9993	7.9993	7.9993	7.9993	7.9993	7.9894	7.9918
Barbara	512 × 512	7.9995	—	—	—	—	7.9898	—
Lena	512 × 512	7.9993	7.9994	—	7.9992	7.9993	—	7.9910
Boats.512	512 × 512	7.9994	—	7.9992	7.9994	7.9991	—	—
Girlface	512 × 512	7.9995	—	—	—	—	—	—
Brain	512 × 512	7.9994	—	—	—	—	—	—
Cameraman	512 × 512	7.9995	—	—	—	—	7.9896	—
Cameraman	256 × 256	7.9973	—	—	—	—	—	—
Lena	256 × 256	7.9975	—	—	—	7.9971	—	—
Girlface	256 × 256	7.9972	—	—	—	—	—	—

Table 5: Outcomes of Local Shannon Entropy.

Images	Size	Cipher Image
Boat.512	512 × 512	7.9019
Barbara	512 × 512	7.9028
Peppers	512 × 512	7.9030
Baboon	512 × 512	7.9034
Brain	512 × 512	7.9027
Cameraman	512 × 512	7.9024
Girlface	256 × 256	7.9024
Cameraman	256 × 256	7.9022
Lena	256 × 256	7.9031

Key sensitivity is a crucial metric for evaluating the robustness of an encryption algorithm [62]. In the proposed algorithm, the parameters of the mHNN model, construction of 2D semi-magic matrix and the configuration parameter of the GQAT considered as an encryption keys. To assess the key sensitivity of the proposed algorithm, a slight perturbation is introduced to the original key values. Specifically, the keys are modified as follows:

$\{x_i(0)\}_{i=1}^3 + \mu$, $a' = a + \mu$, $\omega' = \omega + \mu$ and $c' = c + \omega$, $\mu = 10^{-15}$. Fig. 3 represents the decrypted images constructed from the original and slightly altered keys. A slight change in the key leads to an entirely erroneous decryption, revealing no significant information regarding the plain image. This indicates that the proposed algorithm is highly sensitive to key alteration, hence substantially augmenting its security [63].

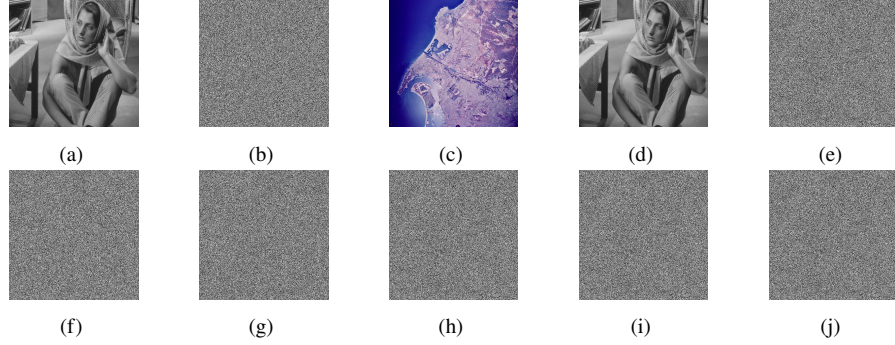


Figure 3: Key sensitivity: (a) original image; (b) encrypted image by key K ; (c) ciphertext image; (d) decrypted image with Key K ; (e)-(j) reconstructed images using Keys K_1 to K_5 .

Correct Key $K = \{\{x_i(0)\}_{i=1}^3, a, b, c, A, k, \omega, i_t, c, d\}$
 Alter Key $K_1 = \{\{x'_i(0)\}_{i=1}^3, a, b, c, A, k, \omega, i_t, c, d\}$
 Alter Key $K_2 = \{\{x'_i(0)\}_{i=1}^3, a, b, c, A, k, \omega, i_t, c, d\}$
 Alter Key $K_3 = \{\{x'_i(0)\}_{i=1}^3, a, b, c, A, k, \omega, i_t, c, d\}$
 Alter Key $K_4 = \{\{x_i(0)\}_{i=1}^3, a', b, c, A, k, \omega, i_t, c, d\}$
 Alter Key $K_4 = \{\{x_i(0)\}_{i=1}^3, a, b, c, A, k, \omega', i_t, c, d\}$
 Alter Key $K_5 = \{\{x_i(0)\}_{i=1}^3, a, b, c, A, k, \omega, i_t, c', d\}$

1.5. Adjacent correlation analysis

The relationship between adjacent pixels in an image can be generated by calculating the horizontal (H), vertical (V), and diagonal (D) correlation coefficients [13]. These coefficients are determined as follows:

$$C_c(p, q) = \frac{\sum_{i=1}^N \left(\left(p_i - \frac{1}{N} \sum_{i=1}^N p_i \right) \left(q_i - \frac{1}{N} \sum_{i=1}^N q_i \right) \right)}{\sqrt{\sum_{i=1}^N \left(p_i - \frac{1}{N} \sum_{i=1}^N p_i \right)^2} \sqrt{\sum_{i=1}^N \left(q_i - \frac{1}{N} \sum_{i=1}^N q_i \right)^2}} \quad (7)$$

where p, q are neighboring pixels and N is the size of image [64]. A total of 5000 pairs of adjacent pixels were randomly picked from both plain and encrypted images to compute the average correlation coefficient values in the H, V, D directions. The outcomes, presented in Table 6, indicate that the encrypted images generated by the propounded algorithm demonstrate negative or near-zero

Table 6: Correlation outcomes of different images

Image	Color	Plain Image			Cipher Image		
		H	V	D	H	V	D
Baboon	Gray	0.9261	0.8689	0.9543	-0.0014	-0.0028	$-4.8114 e^{-04}$
Brain	Gray	0.9905	0.9912	0.9845	-0.0006	-0.0015	0.0003
Peppers	Gray	0.9532	0.9419	0.9610	-0.0004	$-5.2157 e^{-04}$	0.0011
Barbara	Gray	0.8914	0.9612	0.8284	0.0009	$2.8166 e^{-04}$	-0.0021
Boat.512	Gray	0.9582	0.9821	0.9638	$1.3997 e^{-04}$	-0.0069	0.0042
Cameraman	Gray	0.9881	0.9902	0.9686	0.0007	-0.0039	-0.0049
Girlface	Gray	0.9743	0.9777	0.9628	-0.0016	-0.0051	$6.1291 e^{-04}$
Lena	Gray	0.9667	0.9749	0.9812	-0.0095	-0.0084	0.0007
Cameraman	Gray	0.9499	0.9574	0.9814	0.0008	0.0061	$5.5011 e^{-04}$

correlation coefficients, signifying a minimal relationship between adjacent pixels. Moreover, Figure 4 indicates scatter plots that visually represents the pixel correlations. The linear patterns in the scatter plots for the plain images reveal a strong relationship between adjacent pixels, whereas the non-linear patterns for the cipher images reflect a significantly weakened correlation. These results confirm the capability of the proposed algorithm to effectively safeguard information against statistical attacks.

1.6. Differential attacks

The algorithm's resistance to differential attacks is determined by calculating the Number of Pixel Change Rates (NPCR) and the Unified Average Change of Intensity (UACI). The mathematical definition of NPCR nad UACI can be described as follows [51]:

$$\begin{cases} \zeta(u, v) = \begin{cases} 0, & \text{if } S(u, v) = T(u, v) \\ 1, & \text{if } S(u, v) \neq T(u, v) \end{cases} \\ \text{NPCR}(S, T) = \mu = \frac{\sum_{u=1}^M \sum_{v=1}^N \zeta(i, j)}{M \times N} \times 100\% \end{cases} \quad (8)$$

$$\text{UACI}(S, T) = \Psi = \frac{1}{M \times N} \left(\sum_{u=1}^M \sum_{v=1}^N \frac{|S(u, v) - T(u, v)|}{255} \right) \times 100\% \quad (9)$$

where $M \times N$ depicts the size of image, $\zeta(u, v)$ is the difference between two encrypted images S and T . To ensure that an image encryption algorithm meets the required security standards, it must satisfy the condition $\mu_\alpha > \mu_\alpha^*$ and $\Psi \in$

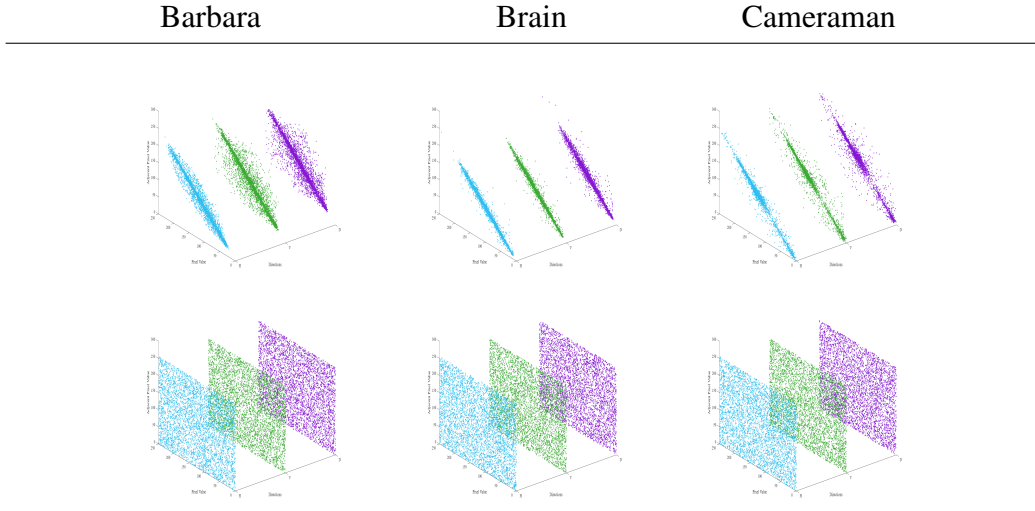


Figure 4: CC plots: first row depicts plain image coefficients in each of three H,V,D directions respectively; second row depicts the corresponding plots for the encrypted image.

$(\Psi_{\alpha}^{*-}, \Psi_{\alpha}^{*+})$, where α denotes the significance level. The proposed algorithm has been evaluated at a significance level of $\alpha = 0.05$.

1.7. Clipping attack analysis

During network transmission, cipher images may be affected by various disturbances such as noise contamination and data loss, which can degrade the quality of the recovered plain image. To evaluate the robustness of the proposed scheme, its performance under cropping attacks (CA) is investigated. In the experiments, the Barbara image is selected as the test case, and different cropping masks are applied to the cipher image to simulate partial data loss. As illustrated in Fig. 5, the reconstructed images remain visually recognizable and semantically meaningful even under severe cropping conditions, demonstrating strong robustness of the proposed algorithm. The corresponding PSNR values reported in Table 8 further validate that satisfactory reconstruction quality is preserved despite these transmission-related interferences.

Table 7: Comparative analysis of $NPCR(\rho)(\%)$ and $UACI(\Phi)(\%)$ values

Theoretical Values of μ^* and Ψ^* [50]									
	256×256	$\mu_{0.05}^* = 0.9957$	$\Psi_{0.05}^{*-} = 0.3328$, $\Psi_{0.05}^{*+} = 0.3364$						
	512×512	$\mu_{0.05}^* = 0.9959$	$\Psi_{0.05}^{*-} = 0.337$, $\Psi_{0.05}^{*+} = 0.3355$						
	1024×1024	$\mu_{0.05}^* = 0.9960$	$\Psi_{0.05}^{*-} = 0.342$, $\Psi_{0.05}^{*+} = 0.3351$						
Calculated values of μ and Ψ									
Image	Proposed algo.		[56]		[57]		[58]		
	μ	Ψ	μ	Ψ	μ	Ψ	μ	Ψ	
Brain	99.607	33.463	–	–	–	–	–	–	–
Barbara	99.598	33.417	99.606	33.426	99.604	33.472	99.607	33.472	
Baboon	99.599	33.403	–	–	–	–	–	–	–
Lena	99.601	33.519	99.616	33.451	–	–	99.611	33.460	
Cameraman	99.588	33.534	–	–	–	–	–	–	–
Peppers	99.603	33.425	99.607	33.432	99.606	33.459	99.608	33.466	
Boat.512	99.585	33.459	–	–	99.607	33.488	99.610	33.472	

Table 8: Occlusion attack metrics: SSIM and PSNR for clipping patterns

Image	Fig.5a		Fig.5b		Fig.5c		Fig.5d		Fig.5e	
	SSIM	PSNR								
Barbara	0.3697	29.9312	0.3370	29.5374	0.3354	29.5415	0.6562	33.1164	0.7082	34.0941
Cameraman	0.4530	29.9533	0.2989	29.2699	0.8995	19.35	0.7229	33.3035	0.7754	34.2426
Brain	0.3141	29.9533	0.2989	29.2699	0.2963	29.5488	0.5987	32.1332	0.6504	33.0544

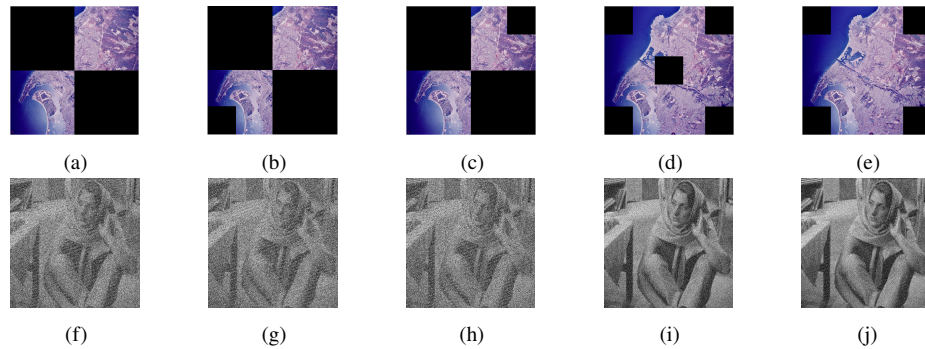


Figure 5: Clipping attack analysis: (a) First row illustrates the different types of occlusion attacks on the ciphertext image; (b) second row depicts the corresponding reconstructed images.

References

- [1] J. Stajic, The future of quantum information processing (2013). [doi:10.1126/science.339.6124.1163](https://doi.org/10.1126/science.339.6124.1163).
- [2] P. Q. Le, F. Dong, K. Hirota, A flexible representation of quantum images for polynomial preparation, image compression, and processing operations, *Quantum Information Processing* 10 (2011) 63–84. [doi:10.1007/s11128-010-0177-y](https://doi.org/10.1007/s11128-010-0177-y).
- [3] Y. Zhang, K. Lu, Y. Gao, M. Wang, Neqr: a novel enhanced quantum representation of digital images, *Quantum information processing* 12 (2013) 2833–2860. [doi:10.1007/s11128-013-0567-z](https://doi.org/10.1007/s11128-013-0567-z).
- [4] H.-S. Li, X. Chen, S. Song, Z. Liao, J. Fang, A block-based quantum image scrambling for gneqr, *IEEE Access* 7 (2019) 138233–138243. [doi:10.1109/ACCESS.2019.2942986](https://doi.org/10.1109/ACCESS.2019.2942986).
- [5] N. Zhou, Y. Hu, L. Gong, G. Li, Quantum image encryption scheme with iterative generalized arnold transforms and quantum image cycle shift operations, *Quantum Information Processing* 16 (2017) 1–23. [doi:10.1007/s11128-017-1612-0](https://doi.org/10.1007/s11128-017-1612-0).
- [6] H.-R. Liang, X.-Y. Tao, N.-R. Zhou, Quantum image encryption based on generalized affine transform and logistic map, *Quantum Information Processing* 15 (2016) 2701–2724. [doi:10.1007/s11128-016-1304-1](https://doi.org/10.1007/s11128-016-1304-1).
- [7] Y.-G. Yang, J. Tian, H. Lei, Y.-H. Zhou, W.-M. Shi, Novel quantum image encryption using one-dimensional quantum cellular automata, *Information Sciences* 345 (2016) 257–270. [doi:10.1016/j.ins.2016.01.078](https://doi.org/10.1016/j.ins.2016.01.078).
- [8] Y. Hu, X. Xie, X. Liu, N. Zhou, Quantum multi-image encryption based on iteration arnold transform with parameters and image correlation decomposition, *International Journal of Theoretical Physics* 56 (2017) 2192–2205. [doi:10.1007/s10773-017-3365-z](https://doi.org/10.1007/s10773-017-3365-z).
- [9] L. Guo, H. Du, D. Huang, A quantum image encryption algorithm based on the feistel structure, *Quantum Information Processing* 21 (2022) 1–18. [doi:10.1007/s11128-021-03364-x](https://doi.org/10.1007/s11128-021-03364-x).

- [10] F. Musanna, S. Kumar, Image encryption using quantum 3d baker map and generalized gray code coupled with fractional chens chaotic system, *Quantum Information Processing* 19 (2020) 1–31. [doi:10.1007/s11128-020-02724-3](https://doi.org/10.1007/s11128-020-02724-3).
- [11] X. Liu, D. Xiao, Y. Xiang, Quantum image encryption using intra and inter bit permutation based on logistic map, *IEEE Access* 7 (2018) 6937–6946. [doi:10.1109/ACCESS.2018.2889896](https://doi.org/10.1109/ACCESS.2018.2889896).
- [12] N. Zhou, W. Chen, X. Yan, Y. Wang, Bit-level quantum color image encryption scheme with quantum cross-exchange operation and hyper-chaotic system, *Quantum Information Processing* 17 (2018) 1–24. [doi:10.1007/s11128-018-1902-1](https://doi.org/10.1007/s11128-018-1902-1).
- [13] N. Zhou, X. Yan, H. Liang, X. Tao, G. Li, Multi-image encryption scheme based on quantum 3d arnold transform and scaled zhongtang chaotic system, *Quantum Information Processing* 17 (2018) 1–36. [doi:10.1007/s11128-018-2104-6](https://doi.org/10.1007/s11128-018-2104-6).
- [14] Q. Lai, L. Yang, G. Chen, Design and performance analysis of discrete memristive hyperchaotic systems with stuffed cube attractors and ultra-boosting behaviors, *IEEE Transactions on Industrial Electronics* 71 (7) (2023) 7819–7828.
- [15] Q. Lai, L. Yang, G. Hu, Z.-H. Guan, H. H.-C. Iu, Constructing multiscroll memristive neural network with local activity memristor and application in image encryption, *IEEE Transactions on Cybernetics* 54 (7) (2024) 4039–4048.
- [16] L. Chua, Memristor-the missing circuit element, *IEEE Transactions on circuit theory* 18 (5) (2003) 507–519.
- [17] M. Di Ventra, Y. V. Pershin, L. O. Chua, Circuit elements with memory: memristors, memcapacitors, and meminductors, *Proceedings of the IEEE* 97 (10) (2009) 1717–1724. [doi:10.1109/JPROC.2009.2021077](https://doi.org/10.1109/JPROC.2009.2021077).
- [18] Q. Deng, C. Wang, Y. Sun, G. Yang, Discrete memristive conservative chaotic map: dynamics, hardware implementation, and application in secure communication, *IEEE Transactions on Cybernetics* (2025).

- [19] S. Zhao, J. H. Chuah, A. S. M. Khairuddin, C. Chen, Single inertial neuron with forced bipolar pulse: chaotic dynamics, circuit implementation, and color image encryption, *Physica Scripta* 100 (1) (2024) 015229.
- [20] C. Fan, Q. Ding, Design and dynamic analysis of a class of new 3-d discrete memristive hyperchaotic maps with multi-type hidden attractors, *Chaos, Solitons & Fractals* 191 (2025) 115905.
- [21] J. J. Hopfield, Neural networks and physical systems with emergent collective computational abilities., *Proceedings of the national academy of sciences* 79 (8) (1982) 2554–2558. [doi:10.1073/pnas.79.8.2554](https://doi.org/10.1073/pnas.79.8.2554).
- [22] U.-P. Wen, K.-M. Lan, H.-S. Shih, A review of hopfield neural networks for solving mathematical programming problems, *European Journal of Operational Research* 198 (3) (2009) 675–687. [doi:10.1016/j.ejor.2008.11.002](https://doi.org/10.1016/j.ejor.2008.11.002).
- [23] P. N. Suganthan, E. K. Teoh, D. P. Mital, Pattern recognition by homomorphic graph matching using hopfield neural networks, *Image and Vision Computing* 13 (1) (1995) 45–60. [doi:10.1016/0262-8856\(95\)91467-R](https://doi.org/10.1016/0262-8856(95)91467-R).
- [24] S. Rbihou, N.-E. Joudar, K. Haddouch, Optimizing parameter settings for hopfield neural networks using reinforcement learning, *Evolving Systems* 15 (6) (2024) 2419–2440. [doi:10.1007/s12530-024-09621-5](https://doi.org/10.1007/s12530-024-09621-5).
- [25] F. Sabahi, M. O. Ahmad, M. Swamy, An unsupervised learning based method for content-based image retrieval using hopfield neural network, in: 2016 2nd international conference of signal processing and intelligent systems (ICSPIS), IEEE, 2016, pp. 1–5. [doi:10.1109/ICSPIS.2016.7869882](https://doi.org/10.1109/ICSPIS.2016.7869882).
- [26] F. Yu, C. Wu, Y. Lin, S. He, W. Yao, S. Cai, J. Jin, Dynamic analysis and hardware implementation of multi-scroll hopfield neural networks with three different memristor synapses, *Nonlinear Dynamics* 112 (14) (2024) 12393–12409. [doi:10.1007/s11071-024-09614-8](https://doi.org/10.1007/s11071-024-09614-8).
- [27] D. S. Jeong, K. M. Kim, S. Kim, B. J. Choi, C. S. Hwang, Memristors for energy-efficient new computing paradigms, *Advanced Electronic Materials* 2 (9) (2016) 1600090. [doi:10.1002aelm.201600090](https://doi.org/10.1002aelm.201600090).

- [28] J. Sun, C. Li, Z. Wang, Y. Wang, A memristive fully connect neural network and application of medical image encryption based on central diffusion algorithm, *IEEE Transactions on Industrial Informatics* 20 (3) (2023) 3778–3788. [doi:10.1109/TII.2023.3312405](https://doi.org/10.1109/TII.2023.3312405).
- [29] F. Yu, X. Kong, W. Yao, J. Zhang, S. Cai, H. Lin, J. Jin, Dynamics analysis, synchronization and fpga implementation of multiscroll hopfield neural networks with non-polynomial memristor, *Chaos, Solitons & Fractals* 179 (2024) 114440.
- [30] H.-M. Dang, H.-M. Yang, D.-H. Jiang, B. Yan, J.-H. Huang, X.-T. Sun, X.-H. Yang, A lsb quantum steganography algorithm based on hash encryption, *Quantum Information Processing* 24 (7) (2025) 210. [doi:10.1007/s11128-025-04818-2](https://doi.org/10.1007/s11128-025-04818-2).
- [31] A. Arumugam, B. Eswaran, L. Ramesh, C. Nallusamy, Quantum-integrated steganography for secure communication using qkd and lsb techniques, in: 2025 International Conference on Electronics and Renewable Systems (ICEARS), IEEE, 2025, pp. 977–983. [doi:10.1109/ICEARS64219.2025.10940779](https://doi.org/10.1109/ICEARS64219.2025.10940779).
- [32] J. Chaharlang, M. Mosleh, S. Rasouli-Heikalabad, A novel quantum steganography-steganalysis system for audio signals, *Multimedia Tools and Applications* 79 (25) (2020) 17551–17577. [doi:10.1007/s11042-020-08694-z](https://doi.org/10.1007/s11042-020-08694-z).
- [33] C. Sutherland, T. A. Brun, Quantum steganography over noisy channels: Achievability and bounds, *Physical Review A* 100 (5) (2019) 052312. [doi:10.1103/PhysRevA.100.052312](https://doi.org/10.1103/PhysRevA.100.052312).
- [34] N. Jiang, N. Zhao, L. Wang, Lsb based quantum image steganography algorithm, *International Journal of Theoretical Physics* 55 (1) (2016) 107–123. [doi:10.1007/s10773-015-2640-0](https://doi.org/10.1007/s10773-015-2640-0).
- [35] M. Naseri, S. Heidari, M. Baghfalaki, R. Gheibi, J. Batle, A. Farouk, A. Habibi, et al., A new secure quantum watermarking scheme, *Optik* 139 (2017) 77–86. [doi:10.1016/j.ijleo.2017.03.091](https://doi.org/10.1016/j.ijleo.2017.03.091).
- [36] J. Sang, S. Wang, Q. Li, Least significant qubit algorithm for quantum images, *Quantum Information Processing* 15 (11) (2016) 4441–4460. [doi:10.1007/s11128-016-1411-z](https://doi.org/10.1007/s11128-016-1411-z).

- [37] S. Heidari, M. R. Pourarian, R. Gheibi, M. Naseri, M. Houshmand, Quantum red–green–blue image steganography, International Journal of Quantum Information 15 (05) (2017) 1750039. [doi:10.1142/S0219749917500393](https://doi.org/10.1142/S0219749917500393).
- [38] N. R. Zhou, T. X. Hua, L. H. Gong, D. J. Pei, Q. H. Liao, Quantum image encryption based on generalized arnold transform and double random-phase encoding, Quantum Information Processing 14 (2015) 1193–1213. [doi:10.1007/s11128-015-0926-z](https://doi.org/10.1007/s11128-015-0926-z).
- [39] S. Ding, N. Wang, H. Bao, B. Chen, H. Wu, Q. Xu, Memristor synapse-coupled piecewise-linear simplified hopfield neural network: Dynamics analysis and circuit implementation, Chaos, Solitons & Fractals 166 (2023) 112899. [doi:10.1016/j.chaos.2022.112899](https://doi.org/10.1016/j.chaos.2022.112899).
- [40] V. M. Vargas, D. Guijo-Rubio, P. A. Gutiérrez, C. Hervás-Martínez, Relu-based activations: Analysis and experimental study for deep learning, in: Conference of the spanish association for artificial intelligence, Springer, 2021, pp. 33–43.
- [41] V. Bhatt, A. Ranjan, An implementation of chua’s circuit employing four-terminal-floating-nullor (ftfn) for secure communications, in: International Conference on Micro/Nanoelectronics Devices, Circuits and Systems, Springer, 2024, pp. 243–253.
- [42] Q. Xu, S. Ding, H. Bao, B. Chen, B. Bao, Activation function effects and simplified implementation for hopfield neural network, Journal of Circuits, Systems and Computers 32 (18) (2023) 2350313. [doi:10.1142/S0218126623503139](https://doi.org/10.1142/S0218126623503139).
- [43] M. Trenkler, A construction of magic cubes, The Mathematical Gazette 84 (499) (2000) 36–41. [doi:10.2307/3621472](https://doi.org/10.2307/3621472).
- [44] N. Rani, V. Mishra, Ways of constructing multiplicative magic cubes, in: International Conference on Frontiers in Industrial and Applied, Springer, 2021, pp. 79–86. [doi:10.1007/978-981-19-7272-0_7](https://doi.org/10.1007/978-981-19-7272-0_7).
- [45] N. Rani, V. Mishra, B. Singh, Piecewise symmetric magic cube: application to text cryptography, Multimedia Tools and Applications 82 (13) (2023) 19369–19391. [doi:10.1007/s11042-022-14153-8](https://doi.org/10.1007/s11042-022-14153-8).

- [46] V. Vedral, A. Barenco, A. Ekert, Quantum networks for elementary arithmetic operations, *Physical Review A* 54 (1) (1996) 147. [doi:10.1103/PhysRevA.54.147](https://doi.org/10.1103/PhysRevA.54.147).
- [47] S. Lloyd, Almost any quantum logic gate is universal, *Physical review letters* 75 (2) (1995) 346. [doi:10.1103/PhysRevLett.75.346](https://doi.org/10.1103/PhysRevLett.75.346).
- [48] L.-H. Gong, X.-T. He, S. Cheng, T.-X. Hua, N.-R. Zhou, Quantum image encryption algorithm based on quantum image xor operations, *International Journal of Theoretical Physics* 55 (2016) 3234–3250. [doi:10.1007/s10773-016-2954-6](https://doi.org/10.1007/s10773-016-2954-6).
- [49] P. Li, Y. Zhao, H. Xiao, M. Cao, An improved quantum watermarking scheme using small-scale quantum circuits and color scrambling, *Quantum Information Processing* 16 (5) (2017) 127. [doi:10.1007/s11128-017-1577-z](https://doi.org/10.1007/s11128-017-1577-z).
- [50] N. Rani, V. Mishra, S. R. Sharma, Image encryption model based on novel magic square with differential encoding and chaotic map, *Nonlinear Dynamics* 111 (3) (2023) 2869–2893. [doi:10.1007/s11071-022-07958-7](https://doi.org/10.1007/s11071-022-07958-7).
- [51] V. Verma, S. Kumar, N. Rani, Novel image encryption algorithm using hybrid 3d-icpcm and hessenberg decomposition, *Nonlinear Dynamics* (2024) 1–27 [doi:10.1007/s11071-024-09620-w](https://doi.org/10.1007/s11071-024-09620-w).
- [52] P. Li, X. Liu, A novel quantum steganography scheme for color images, *International Journal of Quantum Information* 16 (02) (2018) 1850020. [doi:10.1142/S021974991850020X](https://doi.org/10.1142/S021974991850020X).
- [53] H. Xiao, P. Li, Quantum steganography based on reflected gray code for color images, *Intelligent Decision Technologies* 14 (3) (2020) 291–312. [doi:10.3233/IDT-190034](https://doi.org/10.3233/IDT-190034).
- [54] P. Li, A. Lu, Lsb-based steganography using reflected gray code for color quantum images, *International journal of theoretical physics* 57 (5) (2018) 1516–1548. [doi:10.1007/s10773-018-3678-6](https://doi.org/10.1007/s10773-018-3678-6).
- [55] M.-X. Wang, H.-M. Yang, D.-H. Jiang, B. Yan, J.-S. Pan, T. Liu, A novel quantum color image steganography algorithm based on turtle shell and lsb., *Quantum Inf. Process.* 21 (4) (2022) 148. [doi:10.1007/s11128-022-03494-w](https://doi.org/10.1007/s11128-022-03494-w).

- [56] X.-D. Liu, Q.-H. Chen, R.-S. Zhao, G.-Z. Liu, S. Guan, L.-L. Wu, X.-K. Fan, Quantum image encryption algorithm based on four-dimensional chaos, *Frontiers in Physics* 12 (2024) 1230294. [doi:10.3389/fphy.2024.1230294](https://doi.org/10.3389/fphy.2024.1230294).
- [57] M. Hu, J. Li, X. Di, Quantum image encryption scheme based on 2d sine 2-l logistic chaotic map, *Nonlinear Dynamics* 111 (3) (2023) 2815–2839. [doi:10.1007/s11071-022-07942-1](https://doi.org/10.1007/s11071-022-07942-1).
- [58] W. Hao, T. Zhang, X. Chen, X. Zhou, A hybrid negr image encryption cryptosystem using two-dimensional quantum walks and quantum coding, *Signal Processing* 205 (2023) 108890. [doi:10.1016/j.sigpro.2022.108890](https://doi.org/10.1016/j.sigpro.2022.108890).
- [59] S.-X. Jiang, Y. Li, J. Shi, R. Zhang, Double quantum images encryption scheme based on chaotic system, *Chinese Physics B* 33 (4) (2024) 040306. [doi:10.1088/1674-1056/ad1174](https://doi.org/10.1088/1674-1056/ad1174).
- [60] S. Sridharan, G. Ts, R. Amirtharajan, P. Praveenkumar, Quantum scrambling and dna based multilayer image encryption with qtrng and 6d hyperchaotic keys, *Scientific Reports* 15 (1) (2025) 33933. [doi:10.1038/s41598-025-10133-8](https://doi.org/10.1038/s41598-025-10133-8).
- [61] M. Li, X. Song, Y. Zhao, A. A. A. El-Latif, Space-frequency-based multichannel dual encryption for quantum color images using chaotic system and quantum walks, *Quantum Information Processing* 24 (9) (2025) 266. [doi:10.1007/s11128-025-04871-x](https://doi.org/10.1007/s11128-025-04871-x).
- [62] V. Verma, S. Kumar, Quantum image encryption algorithm based on 3d-bnm chaotic map, *Nonlinear Dynamics* (2024) 3829–3855 [doi:10.1007/s11071-024-10403-6](https://doi.org/10.1007/s11071-024-10403-6).
- [63] Z. Zhang, J. Tang, F. Zhang, T. Huang, M. Lu, Medical image encryption based on josephus scrambling and dynamic cross-diffusion for patient privacy security, *IEEE Transactions on Circuits and Systems for Video Technology* (2024). [doi:10.1109/TCSVT.2024.3394951](https://doi.org/10.1109/TCSVT.2024.3394951).
- [64] Y. Zhang, H. Xiang, S. Zhang, L. Liu, Construction of high-dimensional cyclic symmetric chaotic map with one-dimensional chaotic map and its security application, *Multimedia Tools and Applications* 82 (12) (2023) 17715–17740. [doi:10.1007/s11042-022-14044-y](https://doi.org/10.1007/s11042-022-14044-y).